Erzincan Üniversitesi
Fen Bilimleri Enstitüsü Dergisi
2024, 17(3), 650-662
ISSN: 1307-9085, e-ISSN: 2149-4584
Araştırma Makalesi

Erzincan University
Journal of Science and Technology
2024, 17(3), 650-662
DOI: 10.18185/erzifbed.1520178
Research Article

Fabrication of cZIF-67/Ti_3C_2 Nanocomposites As Sulfur Host For Lithium-Sulfur Batteries

Recep YUKSEL[1,2,3*]

[1]Department of Chemistry, Faculty of Science, Eskisehir Osmangazi University (ESOGU), Eskisehir 26040, Türkiye;
[2]Nanoscience and Nanotechnology, Graduate School of Natural and Applied Sciences, Eskisehir Osmangazi University (ESOGU), 26040 Eskisehir, Türkiye;
[3]Advanced Materials Technologies Application and Research Center (IMATEK), Eskisehir Osmangazi University (ESOGU), 26040 Eskisehir, Türkiye.

Received: 22/07/2024, **Revised:** 18/08/2024, **Accepted:** 11/11/2024, **Published:** 31/12/2024

Abstract

It is of great importance to develop high-performance energy storage systems that modern society needs for next-generation technologies such as electric vehicles, consumer electronics, and grid-scale storage. Lithium-sulfur (Li-S) batteries are one of the promising candidates for high-performance energy storage systems due to the high theoretical capacity of the sulfur. On the other hand, some drawbacks, such as the insulating nature of the sulfur and the polysulfide solubility, limit the widespread application of Li-S batteries. Nanocomposite host materials with high surface area and conductive nature can potentially improve the stability of sulfur cathodes. In this study, the MOF-derived heteroatom-doped carbon (cZIF-67) and two-dimensional Ti_3C_2 MXene materials were used to fabricate cZIF-67/Ti_3C_2 nanocomposites. The fabricated cZIF-67/Ti_3C_2 nanocomposites were used as a sulfur host material for Li-S batteries. After the structural and chemical characterizations, S/cZIF-67/Ti_3C_2 nanocomposite cathodes were used in Li-S batteries, and their performance-related properties were examined. The fabricated S/cZIF-67/Ti3C2 cathodes eliminate the adverse effects caused by the insulating nature of sulfur and lithium polysulfides.

Keywords: Energy storage, Lithium-sulfur batteries, MOF, MXene

Lityum-Sülfür Bataryalar İçin Kükürt Tutucu cZIF-67/Ti_3C_2 Nanokompozitlerin Üretimi

Öz

Modern toplumun elektrikli araçlar, tüketici elektroniği ve şebeke tipi depolama gibi yeni nesil teknolojiler için ihtiyaç duyduğu yüksek performanslı enerji depolama sistemlerinin geliştirilmesi büyük önem taşıyor. Lityum-sülfür (Li-S) bataryalar, kükürtün yüksek teorik kapasitesi nedeniyle yüksek performanslı enerji depolama sistemleri için umut verici adaylardan biridir. Öte yandan kükürtün yalıtkan doğası ve polisülfür çözünürlüğü gibi bazı dezavantajlar Li-S bataryaların geniş çaptaki uygulamasını sınırlamaktadır. Yüksek yüzey alanına ve iletken doğaya sahip nanokompozit konak malzemeler, kükürt katotlarının stabilitesini iyileştirme potansiyeline sahiptir. Bu çalışmada, MOF'tan türetilmiş heteroatom katkılı karbon (cZIF-67) ve iki boyutlu Ti_3C_2 MXene malzemeler kullanılarak cZIF-67/Ti_3C_2 nanokompozitleri üretilmiştir. Üretilen cZIF-67/Ti_3C_2 nanokompozitler Li-S bataryalar için kükürt tutucu malzeme olarak kullanıldı. Yapısal ve kimyasal karakterizasyonların ardından S/cZIF-67/Ti_3C_2 nanokompozit katotlar Li-S bataryalarda kullanılarak performans ilintili özellikleri incelenmiştir. Üretilen S/cZIF-67/Ti_3C_2 katotlar ile kükürtün yalıtkan yapısından ve lityum polisülfürlerden kaynaklanan olumsuz etkiler ortadan kaldırılmıştır.

Anahtar Kelimeler: Enerji depolama, Lityum-sülfür bataryalar, MOF, MXene.

*Corresponding Author: recep.yuksel@ogu.edu.tr
Recep YUKSEL, https://orcid.org/0000-0001-8178-0165

1. Introduction

Modern society has an increasing energy demand for new technologies such as electric vehicles, smart buildings, and consumer electronics. This demand has also enhanced the need for sustainable and cost-effective production and storage systems [1, 2]. Thus, a global race exists to develop innovative energy production and storage technologies using low-cost and sustainable technologies. The significant success of lithium-ion batteries (LIBs) over the past thirty years has undoubtedly made them the leading battery technology in developing high-capacity energy storage systems. Due to a series of structural limitations, LIBs cannot meet the requirements of next-generation electric vehicles and grid-scale energy storage systems regarding energy density and cost-effectiveness.

Sulfur (S) is one of the few substances found in elemental form in nature and is the 16th most abundant element in the earth's crust, making it widely available. Additionally, sulfur obtained as a by-product during industrial processes is available in large reserves. Sulfur is a cathode material in lithium-sulfur batteries [3]. Sulfur's theoretical specific capacity is 1675 mAh g^{-1} [4], approximately ten times higher than metal oxide materials commonly used in lithium-ion batteries [5]. All these features show that sulfur is a suitable battery material for developing high-energy-density, low-cost, and sustainable energy systems. Therefore, the emergence of Li-S batteries has generated significant interest in academic and industrial energy storage research.

Lithium-sulfur batteries operate on a significantly different principle from lithium-ion batteries [4]. Li-ion batteries generally use layered or tunnel-type metal oxides ($LiMO_x$) at the positive electrode. Similarly, negative electrode materials also have layered structures. These structures allow Li^+ ions to move reversibly between the positive and negative electrodes during the battery's charge-discharge processes. In Li-S batteries, the energy obtained is based on the reaction of Li^+ with S^{2-}. The following equations clearly demonstrate the electrochemical reaction mechanism of Li-S batteries [6]. During electrochemical discharge, elemental sulfur is reduced to a series of soluble lithium polysulfides (LPS) and some solid-phase polysulfides, which are stored in the cathode electrode (Equation (1)) [3]. During charging, all steps of the discharge process occur in reverse. The reactions at the anode electrode involve Li metal's reversible dissolution and deposition (Equation (2)). The overall reaction of a Li-S cell can be simplified as Equation (3).

Cathode (+): $2e^- + S_8 \leftrightarrow Li_2S_8 \leftrightarrow Li_2S_6 \leftrightarrow Li_2S_4 \leftrightarrow Li_2S_2 \leftrightarrow Li_2S$ (1)

Anode (−): $Li \leftrightarrow Li+ + 2e^-$ (2)

Overall: $S + 2Li^+ + 2e^- \leftrightarrow Li_2S$ (3)

Most scientific studies on Li-S batteries focus on the S cathode. The main challenges in developing LSBs include the insulating nature of sulfur (25 °C, $5*10^{-30}$ S cm^{-1}) and a series of unique problems, such as volume expansion during electrochemical processes. More importantly, the migration of soluble polysulfides from the cathode to the anode during charge/discharge, known as the polysulfide shuttle effect, leads to rapid capacity loss [3, 7].

All these issues result in the inefficient and ineffective use of sulfur, reduced LSB lifespan, and significant capacity losses. Therefore, it is necessary to develop host materials compatible with sulfur and capable of holding it for high-performance LSBs [8].

The performance of electrochemical energy storage systems is closely related to the structural properties of device components. The surface area, pore volume, pore size, and many structural and chemical properties of cathode active materials are significantly correlated. Reports in the literature highlight that porous materials with good conductivity can keep sulfur in the cathode [3, 5]. The most effective approach is physically trapping sulfur within a carbon-based host structure. Due to its environmentally friendly, economical, and easy applicability, melt infiltration is the most commonly used method for depositing sulfur onto host structures [9-11]. The high electronic conductivity of carbon structures ensures more efficient and effective use of insulating sulfur. Therefore, developing new materials with desired structural properties is crucial for high-performance Li-S battery systems.

Zeolitic imidazolate frameworks (ZIFs) are a subgroup of metal-organic frameworks (MOFs) and stand out with their large surface area, crystalline structure, high micropore volume, and chemical stability. Among the MOF structures, ZIF-67 is one of the most studied members. They are formed by the Co-N bonds of cobalt (Co) metal centers with 2-methylimidazole (HMIM) ligands. ZIF-67 MOF demonstrates high micropore volume and specific surface area. However, most MOF structures do not exhibit sufficient ionic and electronic conductivity [8]. Carbon materials derived from MOFs obtained by carbonization are much more conductive. MOF-derived carbon structures can retain the structural features of the parent MOF, such as surface area and pore size, which makes them promising materials for energy storage systems [12]. In the literature, it has been reported that ZIF-67-derived carbon materials are used as sulfur hosts in LSBs [13]. Sulfur cathodes, where sulfur is trapped within the microporous carbon structure obtained by carbonizing ZIF-67, have slowed the diffusion of dissolved polysulfides in Li-S batteries. ZIF-67-derived carbon structures with high sulfur content (59 wt% S) have also shown high electrochemical capacity.

On the other hand, MOF-derived carbon hosts in sulfur cathodes examined so far consist of colloidal particles and are generally sub-micrometer in size. In MOF-derived carbon host structures, electron transfer slows down due to the limited electronic conductivity, reduced diffusion kinetics, and increased contact resistance. All these processes can lead to decreased LSB performance and lifespan.

As mentioned earlier, soluble lithium polysulfide compounds formed during electrochemical processes in Li-S batteries migrate from the cathode electrode section to the anode section, causing significant damage to electrochemical performance and capacity. MOF-derived heteroatom-doped carbon structures' important features are their polar and hydrophilic surfaces [14, 15]. Polar carbon structures, i.e., heteroatom-doped carbon structures, are very effective in retaining LPS formed during electrochemical processes within the carbon host. The good wetting of heteroatom-doped structures with the electrolyte solution significantly enhances the sulfur cathode's performance and the electrolyte's electrochemical stability [16]. Therefore, heteroatom-doped carbon structures are potential candidates for developing Li-S batteries.

While using MOF-derived carbon materials as sulfur host structures is an innovative approach for enhancing the electrochemical performance and lifespan of Li-S batteries, achieving the desired electronic and ionic conductivity values and slowing down reaction kinetics have not yet fully shown the desired performance. Therefore, two-dimensional conductive materials are needed to shorten the ion diffusion distance, increase electronic conductivity, facilitate charge transfer, and form a three-dimensional integrated structure with MOFs.

Due to their unique morphologies, two-dimensional (2D) layered materials with atomic thickness and high conductivity, like graphene and metal chalcogenides, are potential cathode materials for high-capacity Li-S batteries [17]. The high capacity values of $Ti_3C_2T_x$ MXene structures result from both the increased number of electrochemically active regions accessible to lithium-ions and the prevention of ion aggregation between MXene layers during intercalation [18]. Using highly conductive MXene and high surface area porous MOF in a nanocomposite structure may result in high energy density LSBs. Combining the high electronic conductivity of two-dimensional $Ti_3C_2T_x$ MXene and the high micropore volume of MOF (ZIF-67) structures can create a more effective sulfur-hosting cathode framework within a 3D nanocomposite structure. This 3D nanocomposite cathode structure is strongly likely to contribute significantly to Li-S battery performance. This is because the three-dimensional porous network structure increases the charge transfer kinetics while maintaining the electronic conductivity of these electrode materials [19].

In this study, a three-dimensional MOF/MXene-based sulfur-hosting composite cathode fabrication is carried out by combining the favorable properties of MOFs and MXenes to obtain high energy density Li-S batteries. The Li-S batteries designed with the produced three-dimensional composite structures have high charge-discharge efficiency, long lifespan, and high energy density, with cathodes possessing high electrical conductivity, excellent electron transfer capability, charge transfer mobility, and a large surface area.

2. Material and Methods

2.1. Nanocomposite Cathode Fabrication

2.1.1 $Ti_3C_2T_x$ MXene Synthesis:

The Ti_3AlC_2 MAX phase in powder form was obtained from a local seller (Nanografi Co.) and used for the $Ti_3C_2T_x$ MXene synthesis. To etch the atomic layers of Al in Ti_3AlC_2, an acid mixture was prepared by adding 5 grams of LiF salt to 9.0 M HCl acid solution. 3.0 grams of MAX powder were slowly added to 40 ml of the acid mixture and stirred at room temperature (<35 °C) at 350 rpm for 24 hours using a magnetic stirrer. Then, the solution was centrifuged at 3500 rpm for 5 minutes repeatedly with deionized water until the pH is neutral. To obtain a homogeneously distributed colloidal MXene solution, $Ti_3C_2T_x$ MXenes were sonicated in an ultrasonic bath for one hour. Then, the dispersed 2D $Ti_3C_2T_x$ MXene sheets were collected by centrifugation and made into a solution at a 2.0 mg/mL concentration.

2.1.2. ZIF-67/ $Ti_3C_2T_x$ Nanocomposite Material Synthesis:

For ZIF-67/ $Ti_3C_2T_x$ nanocomposite production, a homogeneous solution was obtained by adding cobalt nitrate salt to the MXene solution (2.0 mg/mL) and mixing it at high speed with a magnetic stirrer. Following the adsorption of Co^{2+} ions onto the Ti_3C_2 structures, an organic ligand 2-methylimidazole (2-HMIM) solution was added to the initial solution on the magnetic stirrer and stirred at high speed for another 20 minutes. The molar ratio of Co^{2+} salt to 2-HMIM was set to 1:20 for nanocomposite production. Two different mass ratios of ZIF-67/Ti_3C_2 nanocomposites (1:1, and 3:1) were synthesized. The prepared solution was left overnight without disturbing at room temperature to produce the nanocomposite structure. The obtained MOF/MXene nanocomposite structures were purified by centrifugation to remove unreacted ligand groups and metal salts. The synthesized ZIF-67/Ti_3C_2 nanocomposites were freeze-dried to form an aerogel structure.

2.1.3. Thermal Treatment of ZIF-67/Ti_3C_2 MOF/MXene Nanocomposite Structures:

The synthesized ZIF-67/Ti_3C_2 MOF/MXene nanocomposites were then subjected to thermal treatment in an argon gas flow (100 sccm) at low pressure (<20 mbar) in a split tube furnace. The ZIF-67/Ti_3C_2 structures were thermally treated at 600 °C for 2 hours at a ramping rate of 10 °C/min. The resulting nanocomposites were purified by soaking in 2.0 M HCl acid overnight and then washed with deionized water. The obtained cZIF-67/Ti_3C_2 cMOF/MXene nanocomposite structures were dried in a vacuum oven for 24 hours.

2.1.4. Sulfur Loading into cZIF-67/Ti_3C_2 cMOF/MXene Nanocomposite Structures:

Sulfur was loaded into the cZIF-67/Ti_3C_2 nanocomposite using the melt infiltration method. For this purpose, the synthesized nanocomposite material was mixed with sulfur at a mass ratio of 1:3 and placed in a hydrothermal reactor. The hydrothermal reactor was heated at 155 °C for 12 hours, and then the sulfur-loaded material (S/c- ZIF-67/Ti_3C_2) was removed from the reactor.

2.2. Li-S Battery Fabrication

2.2.1. Preparation of Cathode Electrodes:

The synthesized S/cZIF-67/Ti_3C_2 nanocomposite was mixed with a polymeric binder polyvinylidene difluoride (PVDF) and conductive additive carbon black (CB) with a mass ratio of 8:1:1 in N-methyl-2-pyrrolidone (NMP) solvent to form an ink solution. Dr. Blade coated The prepared ink onto aluminum foil as a thin film. Then, the thin film cathode electrodes were dried at room temperature and kept in a vacuum oven at 60 °C for 24 hours. The prepared thin film cathodes were cut into discs (15 mm in diameter) using a disc cutter and made ready for Li-S battery assembly.

2.2.2. Preparation of Electrolyte for Li-S Batteries:

The electrolyte solution for Li-S batteries was prepared by mixing 1.0 M lithium bis(trifluoromethanesulfonyl)imide (LiTFSI) salt in a 1:1 volume ratio of 1,3-dioxolane (DOL) and dimethoxyethane (DME) solvent mixture with 0.5 M $LiNO_3$ salt additive. The electrolyte preparation processes were carried out in an Argon atmosphere glovebox (O_2 <0.1 ppm and H_2O <0.1 ppm) using a magnetic stirrer and stored in the glovebox.

2.2.3. Li-S Battery Assembly:

The fabricated S/cZIF-67/Ti_3C_2 cathodes and lithium metal foils as anodes were used to assemble 2032 coin-cell Li-S batteries in the glovebox. Commercial Celgard 2400 separators were used to separate the anode and cathode electrodes physically. The electrolyte (μL)/sulfur (mg) ratio for S/cMOF/MXene cathodes was 20 to fabricate Li-S batteries. The fabricated Li-S batteries were rested in ambient conditions for at least 1-2 hours before the electrochemical measurements.

2.3. Characterizations

2.3.1. Structural and Chemical Characterizations:

The structural and chemical characterizations of the fabricated materials and electrodes were done using various methods and techniques. Scanning electron microscopy (SEM) was used to observe the particle size and morphology. X-ray diffraction spectroscopy (XRD) was used for the structural analyses. The BET (Brunauer-Emmett-Teller) method was used to determine the specific surface area. The sulfur content in the nanocomposite structures was determined using thermal gravimetric analysis (TGA).

2.3.2. Electrochemical Characterizations:

The electrochemical performance of the fabricated Li-S batteries was carried out using cyclic voltammetry (CV), galvanostatic charge-discharge (GCD), and cycle life tests. CV measurements were performed in a voltage range of 1.6-2.8 V at scan rates of 0.1-0.5 mV/s. The scan rates were decided based on the position change of sulfur's redox peaks. GCD measurements were performed at 0.1-5.0 C-rates. The 1.0 C-rate was determined based on sulfur's theoretical capacity of 1675 mAh g^{-1} regarding the sulfur amount used in the cathode electrode.

3. Results and Discussion

$Ti_3C_2T_x$ (or Ti_3C_2) MXenes are well-known materials because of their two-dimensional structures and high electronic conductivity. $Ti_3C_2T_x$ MXenes were obtained from the Ti_3AlC_2 MAX phase using the LiF+HCl etching solution. During exfoliation of Ti_3C_2 sheets, 2D sheets form an accordion-like structure and then are dispersed to a homogeneous

solution using an ultrasonic bath. Since MXene structures are decorated with functional groups, they can be distributed by mechanical processes and form a homogeneous solution. The XRD diffraction pattern of the Ti_3C_2 MXene structures produced from the commercially available MAX phase is shown in Figure 1(a). The obtained XRD diffraction pattern is consistent with studies in the literature [20]. The XRD diffraction pattern of Ti_3C_2 indicates that Al layers were successfully removed from the structure.

The SEM image of the produced 2D Ti_3C_2 MXene structures is shown in Figure 1(b). The SEM image shows that MAX phase is etched well and MXene layers are successfully produced. The SEM and corresponding EDS elemental mapping images of the distributed Ti_3C_2 MXene sheets on a silicon substrate are shown in Figures 1(c)-(d). According to the EDS elemental mapping images in Figure 1(d), titanium and carbon are present in Ti_3C_2 MXene. At the same time, oxygen and flor elements originate from the surface functional groups on the Ti_3C_2 MXene sheets.

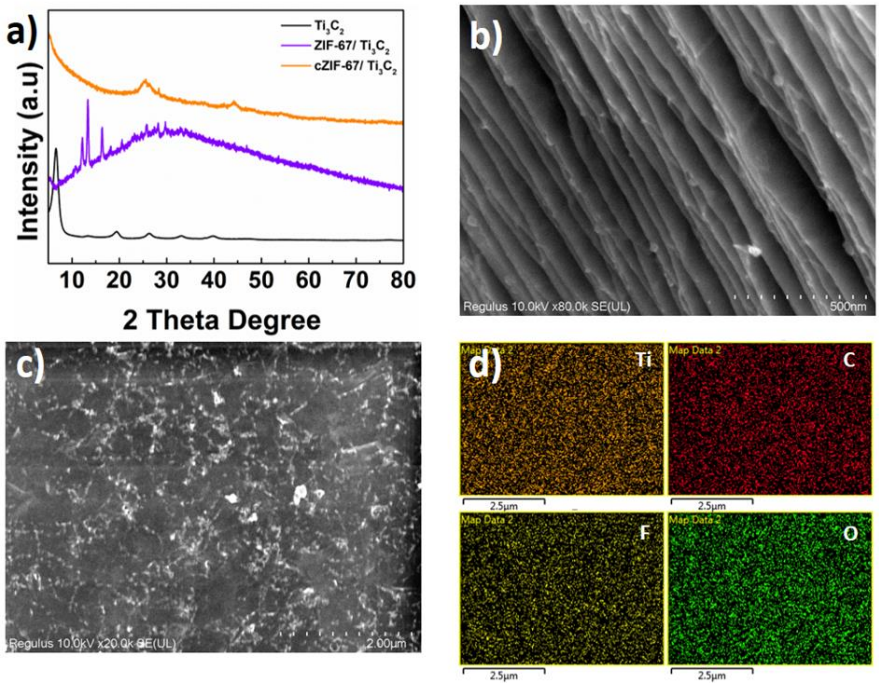

Figure 1. (a) XRD patterns of MXene and ZIF-67/MXene structures. (b)-(c) SEM image of two-dimensional Ti_3C_2 MXenes, and (d) EDS elemental mapping of Ti_3C_2 MXenes.

2D Ti_3C_2 MXenes were combined with ZIF-67 MOFs to form nanocomposite structures. Co^{+2} metal ions were mixed with MXene sheets using a magnetic stirrer, and the Co^{+2} ions were coordinated onto the MXenes. Then, MOF structures were synthesized on MXene layers in a controlled manner with the ligand groups added according to the 1:20 molar metal ion-to-ligand ratio. Three different mass ratios of ZIF-67/Ti_3C_2 nanocomposites (1:1, and 3:1) were synthesized and then carbonized to obtain c-ZIF-67/Ti_3C_2 nanocomposites. Figure 1(a) shows the XRD patterns of the ZIF-67/Ti_3C_2 nanocomposite structure, containing 3:1 mass ratio of ZIF-67 and Ti_3C_2, and the cZIF-67/Ti_3C_2 after the thermal treatment. The XRD pattern of the nanocomposite with 3:1 mass ratio of ZIF-67 and Ti_3C_2 shows characteristic diffraction peaks of ZIF-67. Due to the well-ordered crystalline structure of MOFs, the strong XRD peaks of ZIF-67 were observed. Figure 1(a) shows the

XRD pattern of the thermally treated nanocomposite structure (c-ZIF-67/Ti_3C_2). The functional groups on the surface of the Ti_3C_2 layers are eliminated at 600 °C under argon gas flow, and the ZIF-67 structures are carbonized, transforming into heteroatom (nitrogen)-doped carbon structures. The XRD pattern of the cZIF-67/Ti_3C_2 nanocomposite demonstrates that the diffraction peaks of ZIF-67 are eliminated, and only the carbon-related diffraction pattern is predominantly obtained. The reason for the significant loss of the ZIF-67 crystalline structure peaks in the XRD pattern after carbonization is that the resulting heteroatom-doped carbon structure is slightly graphitic carbons.

The SEM and EDS elemental mapping images of the fabricated nanocomposite containing 1:1 mass ratio ZIF-67/Ti_3C_2 are shown in Figure 2. ZIF-67 particles are synthesized on MXene layers to form a nanocomposite structure. According to the EDS elemental mapping images shown in Figure 2, titanium is only present in MXene, while cobalt, and nitrogen elements are originated from ZIF-67 structures.

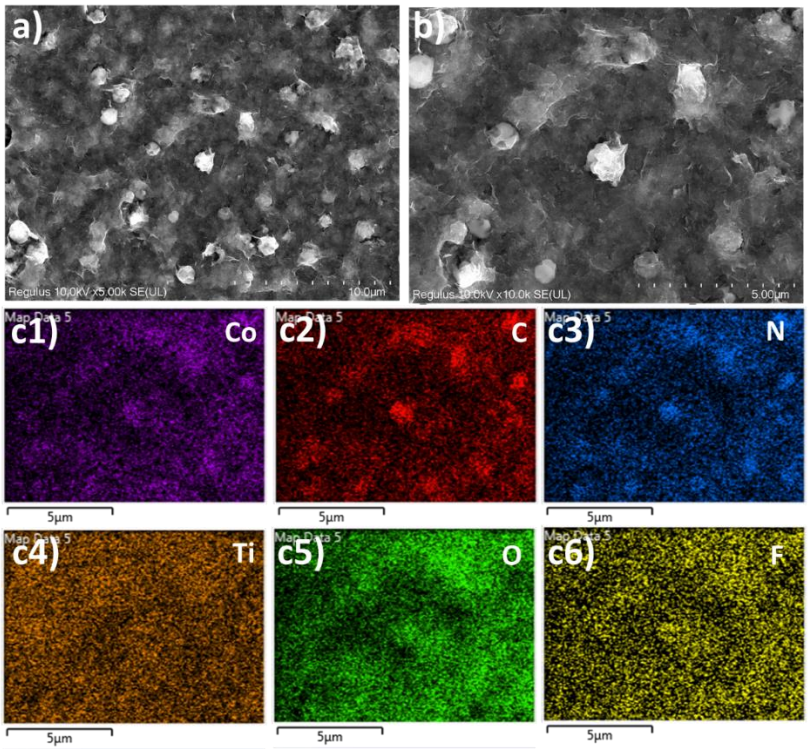

Figure 2. SEM and EDS elemental mapping images of ZIF-67/Ti_3C_2 MXene structures.

Figure 3 shows the SEM and EDS elemental mapping images of the 3:1 cZIF-67/Ti_3C_2 nanocomposite. The SEM images show that the nanocomposite structure has transformed into a three-dimensional porous structure with a high surface area after carbonization. The EDS elemental mapping images show that the samples contain a high amount of nitrogen, indicating that the MOF structures have transformed into carbon structures with a high nitrogen content.

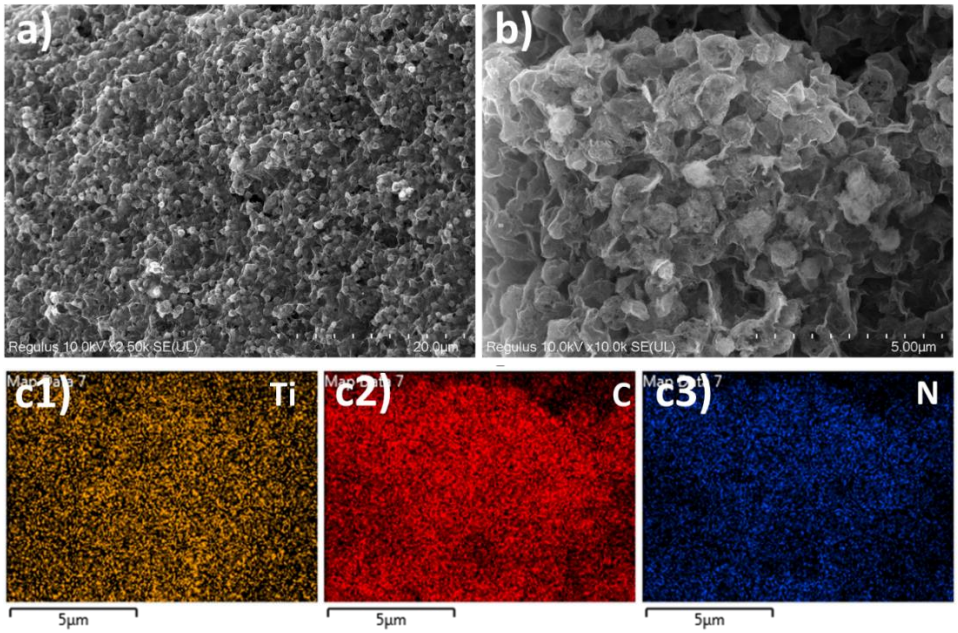

Figure 3. SEM and EDS elemental mapping images of cZIF-67/Ti_3C_2 nanocomposite with 3:1 mass ratio.

Due to the small lateral size and layered structure of MXenes, consisting of three rows of metal and two rows of carbon atoms, they have relatively low specific surface areas than the other 2D materials. On the other hand, the cMOF/MXene structures obtained by nanocomposite formation with two-dimensional MXene and MOF polyhedral particles have high surface areas and pore volumes. Figure 4(a) shows the BET surface area analysis of ZIF-67/MXene nanocomposite structures. The produced ZIF-67/MXene nanocomposite structures with 1:1 and 3:1 ratios have 311 and 340 m^2/g surface areas, respectively.
Sulfur impregnation was performed on the heteroatom-doped cZIF-67/Ti_3C_2 structures via melt fusion method, and the sulfur content in the fabricated S/cZIF-67/Ti_3C_2 was determined by TGA analysis. Figure 4(b) shows the TGA results of the S/cZIF-67/Ti_3C_2 nanocomposite structure. The TGA result shows that cZIF-67/Ti_3C_2 nanocomposites mixed with sulfur at three times their mass contain approximately 75 % sulfur.

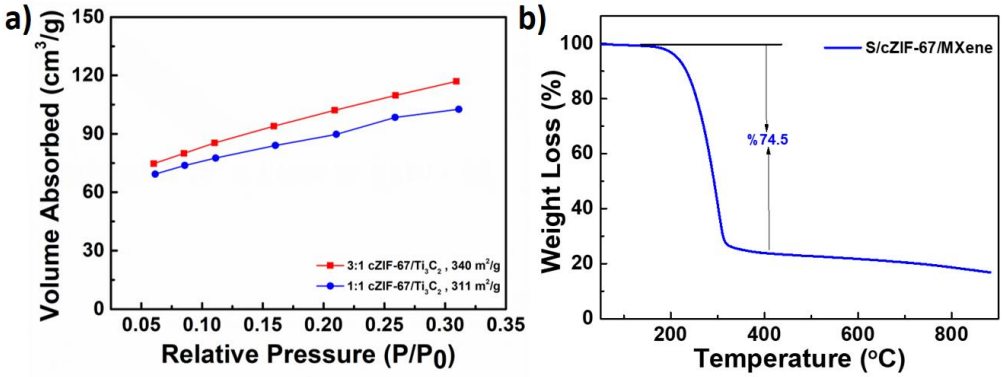

Figure 4. (a) Surface area analysis of ZIF-67/MXene nanocomposite structures. (b) TGA analysis of S/cZIF-67/Ti_3C_2 nanocomposite structures.

Electrochemical energy storage properties of the fabricated cathodes using cZIF-67/Ti_3C_2 nanocomposites with different mass ratios were investigated. Cyclic voltammetry (CV) measurements of the fabricated Li-S cells were done in a voltage window of 1.6-2.8 V. The CV results of the fabricated cathodes at a scan rate of 0.1 mV s^{-1} are shown in Figure 5(a). The oxidation peaks of sulfur are located around 2.4 V, while the reduction peaks are observed around 2.25 and 1.95 V. The fabricated Li-S batteries with the 3:1 mass ratio cZIF-67/Ti_3C_2 nanocomposite have a sharp oxidation peak, while the other nanocomposite shows combined double peaks. CV results of the fabricated S/cZIF-67/Ti_3C_2 cathodes were also obtained at different scan rates and are shown in Figure 5(b). The obtained CV results show that sulfur's oxidation and reduction peaks shift to higher and lower voltage values as the scan rate increases. The results demonstrate that the produced cathode electrodes have reversible electrochemical performance.

To analyze the charge storage mechanism of the fabricated LSBs more clearly, the CV measurements at different scan rates shown in Figure 5(b) were analyzed and are shown in Figure 5(c)-(e). The diffusive and surface capacitive contribution calculations are analyzed using Equations (4) and (5);

$$i = av^b \quad (4)$$

$$i(v)/v^{1/2} = k_1.v + k_2.v^{1/2} \quad (5)$$

where $k_1.v$ indicates that the surface capacitive contribution is dominant, while $k_2.v^{1/2}$ means the diffusion-based contribution is effective. Generally, high surface area materials show a more widespread surface capacitive effect. When the scan rate decreases, diffusion (purple color) processes are effective, while at high scan rates, the surface capacitive (blue color) is dominant. It is seen that the surface capacitive effect is more pronounced at high scan rates, and the diffusion contribution is more significant at low scan rates for the S/cZIF-67/Ti_3C_2 cathodes.

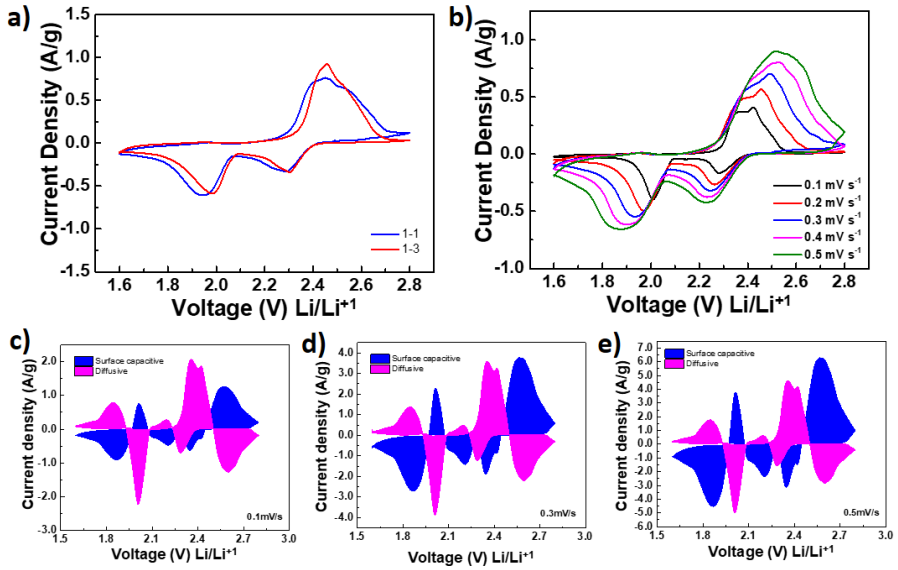

Figure 5. (a) CV measurements of Li-S batteries prepared with S/cZIF-67/Ti_3C_2 cathodes at 0.1 mV/s scan rate. (b) CV measurements of Li-S batteries at different scan rates. (c)-(e) Charge storage mechanism of S/cZIF-67/Ti_3C_2 Li-S battery cathodes.

Figure 6(a)-(b) shows the galvanostatic charge-discharge (GCD) curves of the Li-S batteries at 0.1 C-rate. The fabricated batteries have flat discharge plateaus around 2.3 V and 2.1 V during discharge. Li-S batteries using S/cZIF-67/Ti_3C_2 cathodes reached specific capacity values of approximately 750-780 mAh/g at 0.1 C-rate. GCD measurements were repeated at different C-rates to determine the fabricated Li-S batteries' GCD properties and specific capacities. Figure 6(c) shows the specific capacity change with respect to the C-rate. Battery devices naturally have some capacity drop at high C-rates due to the slow diffusion kinetics. The fabricated Li-S battery devices demonstrated high rate capability at different C-rates. Galvanostatic charge-discharge measurements were also applied to fabricated Li-S batteries at a constant 1.0 C-rate. Figure 6(d) shows the cycle life and capacity retention measurement results at 1.0 C-rate for the fabricated Li-S batteries. After 300 GCD cycles, S cathodes containing 3:1 mass ratio cZIF-67/Ti_3C_2 showed higher electrochemical performance and capacity retention compared to 1:1 mass ratio cZIF-67/Ti_3C_2 cathodes. The obtained results demonstrate that the fabricated nanocomposite structures improved the electrochemical stability and the performance of the Li-S batteries.

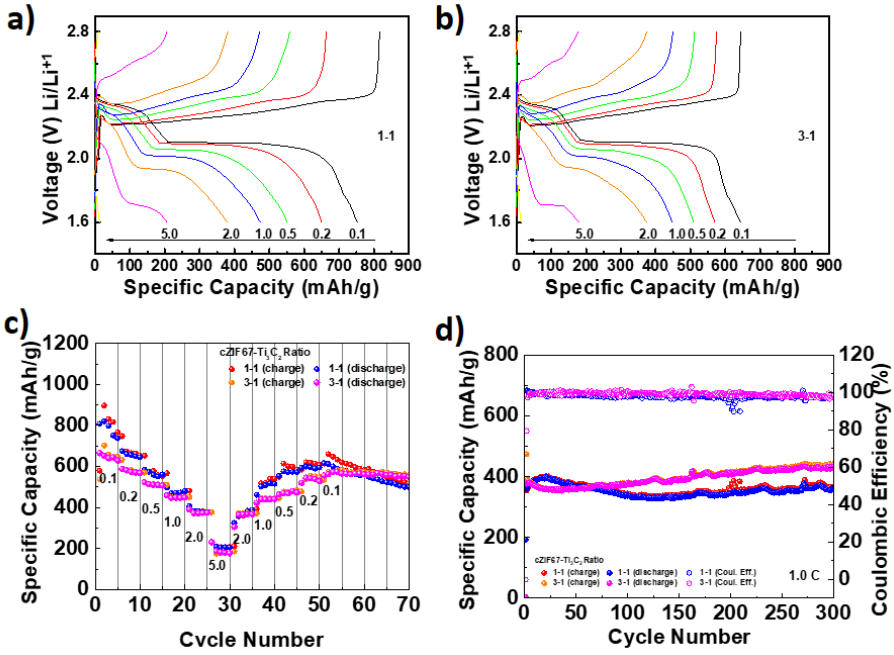

Figure 6. (a)-(b) GCD measurements of the fabricated Li-S batteries with nanocomposite cathodes containing different mass ratios of cZIF-67/Ti_3C_2 at different C-rates. (c) Rate capabilities of the fabricated Li-S batteries. (d) Cycle life and capacity retentions at 1.0 C-rate.

4. Conclusions

cZIF-67/Ti_3C_2 nanocomposite structures with two different mass ratios were synthesized using the wet chemistry method, and their structural characterizations were performed. 3D nanocomposite structures were fabricated by growing high surface area ZIF-67 MOFs on the conductive two-dimensional Ti_3C_2 MXene sheets. The electrochemical charge storage properties of the fabricated Li-S battery devices were carried out using CV and GCD measurements. The fabricated nanocomposite cathodes were found to have potential for use

in Li-S batteries. In GCD measurements, the fabricated Li-S batteries with 1:1 mass ratio S/cZIF-67/Ti_3C_2 cathodes reached a specific capacity of approximately 750 mAh/g. S cathodes containing 3:1 mass ratio cZIF-67/Ti_3C_2 showed higher capacity retention at 1.0 C-rate after 300 GCD cycles. The fabricated cZIF-67/Ti_3C_2 nanocomposite materials demonstrated their potential as a sulfur-host in Li-S batteries with remarkable properties such as high rate capability, capacity retention, and rapid fabrication.

Ethics in Publishing

There are no ethical issues regarding the publication of this study.

Author Contributions

In this study, Recep YUKSEL contributed to scientific literature research, article creation, experimental design, analysis, preparation, and writing of the article results.

Acknowledgments

This study was supported by the Eskişehir Osmangazi University Scientific Research Projects Coordination Unit under project number FBG-2021-1703. The researchers thank the ESOGU BAP coordination for their support.

References

[1] Yuksel, R., et al., Necklace-like Nitrogen-Doped Tubular Carbon 3D Frameworks for Electrochemical Energy Storage. Advanced Functional Materials, 2020. **30**(10): p. 1909725.

[2] Yuksel, R., et al., Metal-Organic Framework Integrated Anodes for Aqueous Zinc-Ion Batteries. Advanced Energy Materials, 2020. **10**(16).

[3] Pang, Q., et al., Advances in lithium–sulfur batteries based on multifunctional cathodes and electrolytes. Nature Energy, 2016. **1**(9): p. 16132.

[4] Huang, L., et al., Electrode Design for Lithium–Sulfur Batteries: Problems and Solutions. Advanced Functional Materials, 2020. **30**(22): p. 1910375.

[5] Fang, R., et al., More Reliable Lithium-Sulfur Batteries: Status, Solutions and Prospects. Advanced Materials, 2017. **29**(48): p. 1606823.

[6] Boyd, D.A., Sulfur and its role in modern materials science. Angewandte Chemie International Edition, 2016. **55**(50): p. 15486-15502.

[7] Qiu, T., et al., Metal–Organic Framework-Based Materials for Energy Conversion and Storage. ACS Energy Letters, 2020. **5**(2): p. 520-532.

[8] Rana, M., et al., Oriented nanoporous MOFs to mitigate polysulfides migration in lithium-sulfur batteries. Nano Energy, 2020. **75**: p. 105009.

[9] Ji, X., K.T. Lee, and L.F. Nazar, A highly ordered nanostructured carbon–sulphur cathode for lithium–sulphur batteries. Nature Materials, 2009. **8**(6): p. 500-506.

[10] Kim, H., et al., Synthesis of three-dimensionally interconnected sulfur-rich polymers for cathode materials of high-rate lithium–sulfur batteries. Nature Communications, 2015. **6**(1): p. 7278.

[11] Seo, S.-D., et al., "Brain-Coral-Like" Mesoporous Hollow CoS2@N-Doped Graphitic Carbon Nanoshells as Efficient Sulfur Reservoirs for Lithium–Sulfur Batteries. Advanced Functional Materials, 2019. **29**(38): p. 1903712.
[12] Wang, H., et al., Metal-organic frameworks for energy applications. Chem, 2017. **2**(1): p. 52-80.
[13] Li, G., et al., A microporous carbon derived from metal-organic frameworks for long-life lithium sulfur batteries. International Journal of Energy Research, 2020. **44**(3): p. 2126-2136.
[14] Guan, B., et al., Blocking Polysulfide with Co2B@ CNT via "Synergetic Adsorptive Effect" toward Ultrahigh-Rate Capability and Robust Lithium–Sulfur Battery. ACS nano, 2019. **13**(6): p. 6742-6750.
[15] Yuksel, R., et al., Necklace-like Nitrogen-Doped Tubular Carbon 3D Frameworks for Electrochemical Energy Storage. Advanced Functional Materials, 2020. **30**(10).
[16] Zhao, M., et al., A Perspective toward Practical Lithium–Sulfur Batteries. ACS Central Science, 2020. **6**(7): p. 1095-1104.
[17] Li, K., et al., 3D MXene Architectures for Efficient Energy Storage and Conversion. Advanced Functional Materials, 2020. **30**(47): p. 2000842.
[18] Liang, X., A. Garsuch, and L.F. Nazar, Sulfur cathodes based on conductive MXene nanosheets for high-performance lithium–sulfur batteries. Angewandte Chemie, 2015. **127**(13): p. 3979-3983.
[19] Zhao, Q., et al., 2D MXene nanosheets enable small-sulfur electrodes to be flexible for lithium–sulfur batteries. Nanoscale, 2019. **11**(17): p. 8442-8448.
[20] Naguib, M., et al., Two-Dimensional Nanocrystals Produced by Exfoliation of Ti3AlC2. Advanced Materials, 2011. **23**(37): p. 4248-4253.